Induction of muscle regeneration by RNA-mediated mitochondrial restoration

Article *in* The FASEB Journal · July 2012

DOI: 10.1096/fj.11-203232

2 authors, including:

Sukanta Jash
Harvard University
33 PUBLICATIONS **203** CITATIONS

SEE PROFILE

The FASEB Journal article fj.11-203232. Published online July 2, 2012.

The FASEB Journal • Research Communication

Induction of muscle regeneration by RNA-mediated mitochondrial restoration

Sukanta Jash and Samit Adhya[1]

Genetic Engineering Laboratory, Indian Institute of Chemical Biology, Council of Scientific and Industrial Research (CSIR), Calcutta, India

ABSTRACT **Skeletal muscle injury is associated with general down-regulation of mitochondrial function. Postinjury regeneration of skeletal muscle occurs through activation, proliferation, and differentiation of resident stem cells, including satellite cells and endothelial precursor cells. We wanted to determine the role of mitochondrial function in the regeneration process. Using a previously described method for complex-mediated delivery to intracellular mitochondria, a combination of polycistronic RNAs encoding the H strand of the rat mitochondrial genome was administered to injured rat quadriceps muscle, resulting in restoration of mitochondrial mRNA levels, organellar translation, and respiratory capacity. Intramuscular ATP levels were elevated on pcRNA treatment of injured muscle; concomitantly, levels of reactive oxygen species in the injured muscle were reduced. These effects combined to produce a notable increase in the rate of wound resolution, accompanied by reduction of fibrosis and acceleration of myogenesis, vasculogenesis, and resumption of muscle contractile function. There was evidence of proliferation of Pax7$^+$ satellite cells, expression of muscle-specific regulatory factors in a specific time sequence, and formation of new myofibers in the regenerating muscle. RNA-induced wound resolution and satellite cell proliferation were sensitive to mitochondrial inhibitors, indicating the importance of oxidative phosphorylation. These results highlight the activation of endogenous stem cells through mitochondrial restoration as a possible alternative to implantation of cultured stem cells.—Jash, S., Adhya, S. Induction of muscle regeneration by RNA-mediated mitochondrial restoration. *FASEB J.* 26, 000–000 (2012). www.fasebj.org**

Key Words: satellite cells · gene delivery · ATP · ROS · myogenesis

As the primary cellular generators of ATP through oxidative phosphorylation (oxphos), as well as of toxic reactive oxygen species (ROS), mitochondria are believed to play a critical role in the origin of, and the recovery from, a variety of human diseases, disabilities, and traumas. Mitochondrial dysfunction has been linked to various forms of tissue injury. In a burn injury model, there was extensive down-regulation of genes involved in oxphos, pyruvate metabolism, citric acid cycle, and glycolysis (1). The muscle respiratory capacity of patients with burn injury is significantly reduced compared to controls (2). Cardiac ischemia is accompanied by decreased functioning of the oxphos apparatus, and paradoxically, electron transport inhibitors protect against injury during reperfusion following ischemia, suggesting that mitochondrial electron transport in the ischemic environment exacerbates injury, possibly through production of ROS (3). Mitochondria are also the prime targets of hepatotoxic drugs, with damaged mitochondria activating cell death pathways (4). In bupivacaine-injured muscle, mitochondrial function is significantly inhibited but is restored to normal levels during regeneration through mitochondrial biogenesis (5). Therefore it appears that, on the one hand, mitochondrial dysfunction can result in injury (liver cirrhosis), while on the other, injury can lead to mitochondrial dysfunction (burn), and furthermore, that mitochondrial up-regulation is associated with the wound-healing process.

Tissue regeneration involves the proliferation and differentiation of resident stem cells. Mitochondrial organization and function are linked with proliferation and/or differentiation of embryonic stem cells (ESCs) as well as other adult stem cells (6–9) and declines during aging (10). Induced pluripotent stem cells

Abbreviations: AF, Alexa Fluor; AntA, antimycin A; CCCP, *m*-chlorocarbonylcyanide phenylhydrazone; eMHC, embryonic myosin heavy chain; ESC, embryonic stem cell; FACS, fluorescence-activated cell sorting; FBS, fetal bovine serum; ICF, isometric contraction force; iPSC, induced pluripotent stem cell; MHC, myosin heavy chain; MRF, myogenic regulatory factor; mtDNA, mitochondrial DNA; Myog, myogenin; oxphos, oxidative phosphorylation; PBS, phosphate buffered saline; PCNA, proliferating cell nuclear antigen; PCR, polymerase chain reaction; pcRNA, polycistronic RNA; PMSF, phenyl methyl sulfonyl fluoride; RIC, RNA import complex; ROS, reactive oxygen species; RT-PCR, reverse transcription-polymerase chain reaction TnT, troponin T; TnT(f), troponin T fast variant; TnT(s), troponin T slow variant; TR, Texas Red

[1] Correspondence: Genetic Engineering Laboratory, Indian Institute of Chemical Biology, 4 Raja S. C. Mullick Rd., Calcutta 700032, India. E-mail: nilugrandson@gmail.com

doi: 10.1096/fj.11-203232

This article includes supplemental data. Please visit *http://www.fasebj.org* to obtain this information.

(iPSCs) have low mitochondrial activity, relying predominantly on glycolysis for ATP generation and maintenance of the dedifferentiated state, while differentiation is accompanied by increased mitochondrial activity (11, 12). Mitochondrial activity may also be critical for the differentiation of satellite cells; studies with cultured myoblasts using mitochondrial inhibitors indicate a role of mitochondrial function in myoblast fusion to myotubes and in the expression of late myogenic markers, such as creatine kinase and troponin-I (13).

Stem cell therapy is being currently studied for its efficacy as a wound-healing agent. The main problems of current methods of stem cell therapy of myocardial infarction are that the endogenous repair rate is low and the implanted cardiac stem cells are unable to repair the lesion (14). Implantation of $CD34^+$ or $CD133^+$ cells leads to slow and incomplete muscle regeneration (15). It is unknown whether deficiencies are related to the low mitochondrial capacity of these cells, and whether modulation of mitochondrial activity would have significant effects on the pathological development and/or resolution of injury.

Previous work from this laboratory has described a novel protocol for transformation of cell and tissue mitochondria with functional RNAs encoding organelle-encoded sequences, both *in vitro* and *in vivo*. The method is based on the mitochondriotropism of a multisubunit RNA import complex (RIC); *i.e.*, its ability to be taken by cells and transported to mitochondria (16). A single polycistronic RNA (pcRNA) encoding a part of the organelle genome restored the respiration of mutant mitochondria harboring a patient-derived mitochondrial DNA (mtDNA) deletion (17). In cells containing multiple mtDNA deletions, a combination of pcRNAs together encoding the entire H-strand protein-coding region (see **Fig. 1*A***) restored respiration and suppressed ROS production (18). Moreover, RNA could be delivered intramuscularly to rats to produce up-regulation of respiratory capacity (19). Using this protocol, we have herein attempted to restore the mitochondrial mRNA levels and function in injured muscle. We found that, as a result, the process of tissue regeneration was significantly accelerated. Thus, mitochondrial restoration may be an effective way to promote rapid wound healing.

MATERIALS AND METHODS

Rat model

Sprague-Dawley rats (male, ~1 yr) were anesthetized with ketamine hydrochloride (100 μl/100 g body wt) before piercing the hindlimb quadriceps muscle 70–80 times with a 26-gauge hypodermic needle (going in ~5 cm) at an angle of ~45° to the longitudinal axis of the fiber. We estimate that ~3000 fibers are damaged at each insertion. The circumference of the lesion was measured at 24-h intervals. All experiments involving animals were carried out according to the guidelines of the Animal Ethics Committee, Indian Institute of Chemical Biology.

Preparation of RNA

Details of the preparation of signal-tagged RNAs have been described previously (17). Briefly, selected regions of rat mtDNA (see Fig. 1) containing one or more protein-coding genes were amplified by polymerase chain reaction (PCR) and ligated to a promoter tag cassette containing a T7 polymerase promoter sequence followed by the D domain of *Leishmania* $tRNA^{Tyr}$ that constitutes a binding site in the RIC-derived carrier complex (20). The resultant DNA was transcribed with T7 RNA polymerase, and the RNA was purified by ethanol precipitation. For microscopy, the RNA was labeled by including Alexa Fluor (AF) 488-or BODIPY-Texas Red (TR)-conjugated uridine triphosphate (Invitrogen, Carlsbad, CA, USA) in the transcription reaction, as described previously (16). pcRNAs 1R, 2R, and 3R contain protein-coding (see Fig. 1*A*) and tRNA genes from contiguous regions of rat mtDNA (19).

Preparation of carrier complex

R6 is a subcomplex of the native *Leishmania tropica* tRIC containing all the essential nucleus-encoded subunits: RIC1, RIC4A, RIC6, RIC8A, RIC8B, and RIC9, and is active for tRNA import (20). The individual subunits were expressed in *Escherichia coli*, purified, and combined *in vitro* to assemble R6, as described previously (20).

RNA treatment

Commonly, a mixture of rat-derived pcRNA 1, 2, and 3 (1 pmol each) was incubated with R6 (20 ng of each subunit) in binding buffer for 30 min on ice to allow RNA-protein (RNP) complex formation, as described elsewhere (17). The RNP was then diluted to 0.1–0.2 ml with phosphate buffered saline (PBS) and injected directly into the injury site.

Subcellular fractionation

Quadriceps muscle mitochondria were prepared by differential centrifugation (21).

In vitro translation

A freshly isolated muscle mitochondrial fraction was incubated with a translation cocktail containing ^{35}S-methionine and other amino acids and cofactors. Translation products were resolved by SDS-PAGE and visualized by fluorography (22).

O_2 uptake measurements

Oxygen consumption by permeabilized muscle preparations was measured in a Hansatech oxygraph (Hansatech, Norfolk, UK) under state 3 respiration conditions, as described elsewhere (23).

ATP estimation

Freshly dissected muscle (0.5 g) was frozen on dry ice, broken into small pieces, and added to 2.5 ml of ice-cold perchloric acid, then homogenized with a precooled glass homogenizer, and the homogenate was centrifuged at 1500 *g* for 20 min. The supernatant (1 ml) was neutralized with 0.14 ml of

neutralizing agent (0.5 M triethanolamine, 2 M K_2CO_3) for 10 min on ice, then centrifuged at 1500 *g* for 20 min. The supernatant was used for estimating ATP using the ATP Bioluminescence Assay Kit (Sigma-Aldrich, St. Louis, MO, USA), as follows: 1 μl supernatant was incubated with 50 μl of luciferin-luciferase assay mix in a total volume of 1 ml for 30 s on ice in the dark, followed by measurement of the luminescence in a Modulus luminometer (Turner Biosystems, Madison, WI, USA).

RNA and DNA analysis

Northern blots of mitochondrial RNA on Hybond N (GE Healthcare, Piscataway, NJ, USA) were probed with the indicated 5′-^{32}P-labeled antisense oligonucleotide (19). Semiquantitative reverse transcription-PCR (RT-PCR) was carried out on 1.5 μg of muscle mitochondrial RNA, using gene-specific sense and antisense primers, as described previously (16); the amount of template was determined to be within the linear range of amplification by titration with normal rat mitochondrial RNA (data not shown). Southern blots of muscle DNA (0.5 μg) digested with *Bgl*II were probed with indicated 5′-^{32}P-labeled antisense oligonucleotides.

Western blots

Muscle fragments were homogenized in 1 ml of ice-cold lysis buffer [20 mM HEPES, 0.2 mM EDTA, 1.5 mM $MgCl_2$, 100 mM NaCl, 1 mM sodium vanadate, 2 mM dithiothreitol, and 0.4 mM phenylmethyl sulfonyl fluoride (PMSF)], supplemented with 0.01 vol of protease inhibitor cocktail (Merck & Co., Whitehouse Station, NJ, USA) for 60 min at 4°C, and centrifuged at 10,000 *g* for 10 min. The supernatant was mixed with 1 ml more of lysis buffer, incubated a further 30 min, and spun at 13,000 rpm for 15 min. The clarified supernatant was concentrated 10-fold in a Microcon 10 centrifugal ultrafilter (Amicon Corp., Danvers, MA, USA), mixed with 5× SDS-PAGE sample buffer and frozen at −80°C until use. Blocked Western blots of 50 μg protein on Hybond C (GE Healthcare) membranes were incubated overnight first with the appropriate primary antibody, then with HRP-conjugated secondary antibody (1:10,000) for 1 h. Bands were detected using the ECL Western blot detection kit (GE Healthcare) by autoradiography.

Preparation and analysis of satellite cells

Muscle fragments (~50 mg) were incubated in DMEM containing 2% (w/v) of type II collagenase for 2 h at 37°C with occasional manual agitation; washed with Ham's F10 nutrient mixture (Invitrogen) containing 20% fetal bovine serum (FBS), 5 ng/ml bovine fibroblast growth factor (FGF), and 1% penicillin-streptomycin; dissociated into fibers by repeated trituration; separated from cell debris by sedimentation under gravity; and washed multiple times. Washed fibers were suspended in growth medium, and satellite cells were liberated by further digestion in PBS containing 2 U/ml dispase and 38 U/ml collagenase for 1 h at 37°C with shaking. After centrifugation at 200 rpm for 2 min to separate fiber debris, the supernatant was mixed with DMEM containing 20% FBS, filtered through a 50-μm mesh, and centrifuged at 1000 rpm for 5 min to collect the mononuclear cell fraction. The cells were fixed, permeabilized and stained sequentially with anti-Pax7 antibody (1:250) plus AF 488-conjugated anti-IgG (Invitrogen) followed by anti-proliferating cell nuclear antigen (PCNA) antibody plus AF 633-conjugated anti-IgG. Samples were analyzed by fluorescence-activated cell sorting (FACS) in a FACS Aria cell sorter (BD Biosciences, San Jose, CA, USA).

Inhibitors

A single dose of *m*-chlorocarbonylcyanide phenylhydrazone (CCCP; 100 μM) or antimycin A (AntA, 100 μM) was injected in 0.1 ml at the wound site 3 h following administration of pcRNA.

Fluorescence microscopy

Fixed and permeabilized muscle cryosections were incubated with appropriate combinations of primary antibody and secondary antibody labeled with AF 395 (blue), AF 488 (green), or AF 633 (red). Sections were DAPI-stained before mounting. Samples were imaged in an A1R confocal microscope using 404-, 488-, and 627-nm lasers and NIS Elements software (Nikon, Tokyo, Japan). For measurement of ROS, muscle cryosections were equilibrated with aerated Ringer's solution at 37°C for 10 min, then incubated with 1 μM MitoSox Red (Invitrogen) for 10 min at 37°C, washed with Ringer's solution, imaged, and quantified as region of interest-based fluorescence intensity/field (n=10). Angiogenesis was estimated by confocal imaging of sections stained with 40 μg/ml FITC-conjugated isolectin B4 (Sigma-Aldrich), which binds to endothelial cells (24). The fluorescence intensity in individual fields (n=10), representing capillary density, was measured as the mean pixel density using the histogram analysis option of Adobe Photoshop 7 (Adobe Systems, San Jose, CA, USA).

Histological examination

To estimate myogenesis, sections from wound tissue were stained with hematoxylin and eosin, and 10–20 random ×40 fields within the wound area were examined for the presence of mature (with peripheral nuclei) or immature (with non-peripheral or central nuclei) fibers. The number of immature fibers per square millimeter is an indicator of myogenesis. Fibrosis was assessed by Accustain trichrome stain (Masson; Sigma-Aldrich) according to the manufacturer's protocol and expressed as the fraction of the area of individual fields (n=10) with collagen deposits, estimated with ImageJ 1.45 software (U.S. National Institutes of Health, Bethesda, MD, USA).

Measurement of isometric contraction force (ICF)

Rat quadriceps muscles with intact tendons were dissected and placed in a Radnoti Tissue-Organ Bath (AdInstruments, Colorado Springs, CO, USA) filled with oxygenated mammalian Ringer solution containing 120.5 mM NaCl, 20.4 mM $NaHCO_3$, 10 mM glucose, 4.8 mM KCl, 1.6 mM $CaCl_2$, 1.2 mM $MgSO_4$, and 1.2 mM NaH_2PO_4, adjusted to pH 7.4 and maintained at 24–25°C. The muscle was gently stretched (not overstretched), and a silk suture was tied to the proximal and distal tendons during dissection and used to attach the muscle to the isometric transducer (TRI201AD; AdInstruments). The muscle length was adjusted very carefully and in small increments to achieve the optimal isometric tension of 2 g (muscles are adjusted to the optimum length (L_o) for the development of isometric twitch force), then rested for at least 20 min before applying contractile voltage. The muscles were stimulated by the electronic field stimulator (1001; AdInstruments) between 2 platinum electrodes placed longitudinally on either side of the muscle (sine wave pulses 10 V,

1-ms duration, frequency 20 Hz, for 625 ms). The muscle was stimulated with a single electrical pulse of different voltages to produce twitch responses. Stimulation voltage is that which produces the maximum twitch response. Data were recorded and analyzed using LabChart 7 software (AdInstruments).

Statistical analysis

Mean ± SD values ($n \geq 3$) were computed wherever indicated.

RESULTS

Restoration of muscle mitochondrial function by a cocktail of RNAs

In our transformation protocol (17), T7 RNA polymerase transcripts of selected stretches of mtDNA are 5′-tagged with a RNA hairpin containing a tRNA import signal that is bound with high affinity to subunit RIC1 of the carrier complex R6, a functional derivative of native RIC (ref. 20 and Fig. 1*A*). Injection of AF 488-labeled RNA into injured muscle resulted in the uptake of the RNA into myofibers near the injury site and in the cytoplasm of fiber-attached satellite cells, and in the colocalization of the internalized RNA after 6 h with myotubular mitochondria (Fig. 1*B*). BODIPY-TR-labeled pcRNA2 was also detected in clusters of $Pax7^+$ satellite cells between myofibers (Fig. 1*C* and Supplemental Fig.S1). Greater than 90% of the $Pax7^+$ cells in these clusters were also RNA^+, indicating high transfection efficiency. As a control, we injected the 23-nt signal tag (D-arm RNA) which is delivered to mitochondria by RIC but has no effect on mitochondrial function (25). Labeled D-arm RNA was also detected within $Pax7^+$ cells (Supplemental Figs.S2 and S3), but the numbers were lower (Fig. 1*C*, right panel); the larger numbers of such cells in pcRNA-treated muscle reflect satellite cell proliferation (see below).

In muscle mitochondria isolated from injured rats treated with pcRNA2, the intact RNA (6.7 kb) was detectable by Northern blot (Fig. 1*D*). In addition, the pcRNA2-encoded CYB mRNA was present at an en-

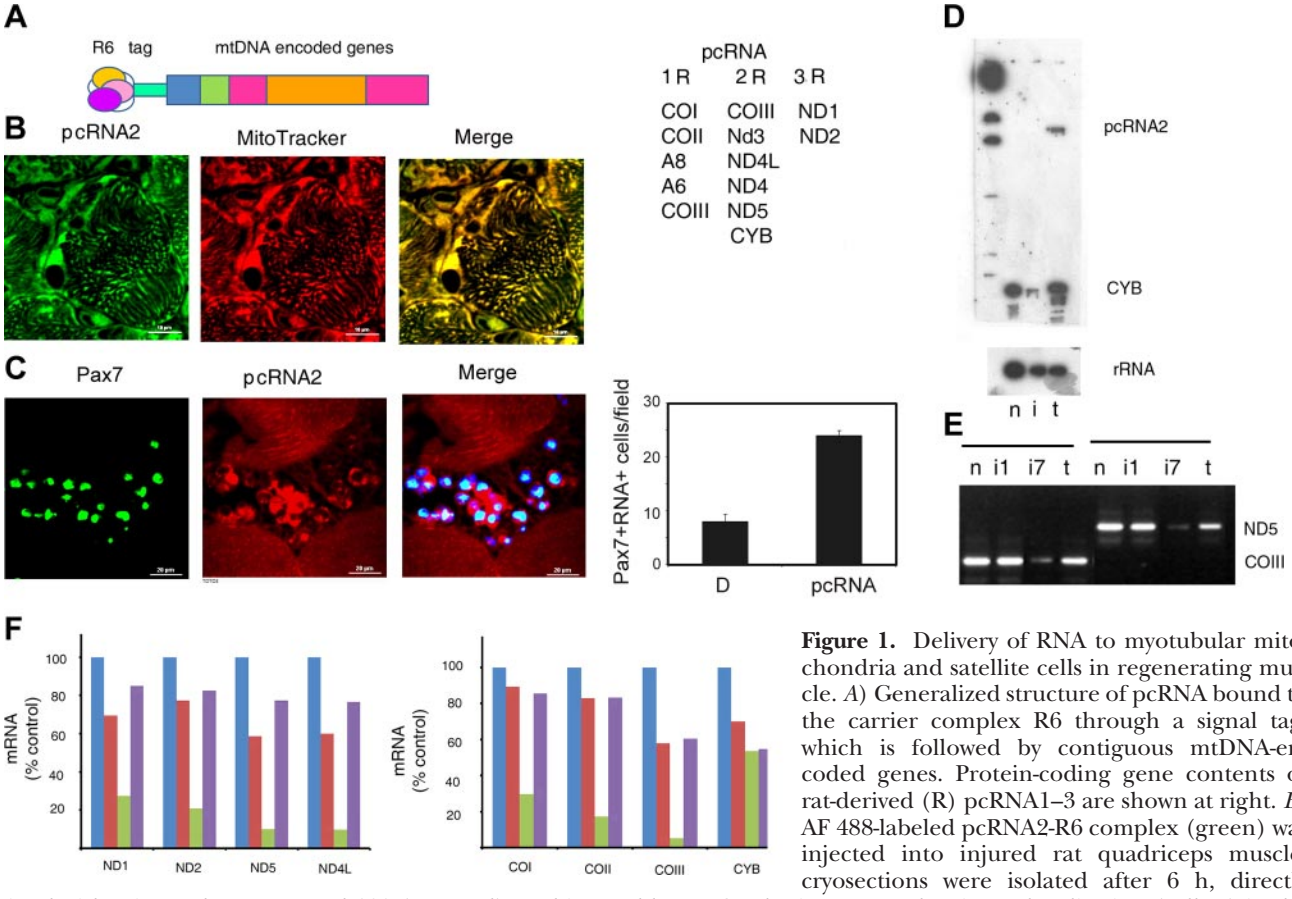

Figure 1. Delivery of RNA to myotubular mitochondria and satellite cells in regenerating muscle. *A*) Generalized structure of pcRNA bound to the carrier complex R6 through a signal tag, which is followed by contiguous mtDNA-encoded genes. Protein-coding gene contents of rat-derived (R) pcRNA1–3 are shown at right. *B*) AF 488-labeled pcRNA2-R6 complex (green) was injected into injured rat quadriceps muscle; cryosections were isolated after 6 h, directly stained with Mitotracker Deep Red 633 (MT; red), and imaged by confocal microscopy, showing colocalization (yellow) in the merged image. Scale bars = 20 μm. *C*) Left panels: $Pax7^+$ satellite cells (green nuclei) containing cytoplasmic BODIPY-TR-labeled pcRNA2 (red) in injured muscle treated with RNA for 12 h. Right panel: quantification of $Pax7^+RNA^+$ cells in injured muscle treated with control D-arm RNA, or with pcRNA1-3. *D*) Northern blot of quadriceps muscle mitochondria from normal rat (lane n), injured rat (lane i), or injured rat treated with pcRNA2-R6 complex for 6 h (lane t), probed with anti-CYB (top) or anti-16 S rRNA (bottom) oligonucleotide. *E*) RT-PCR of mitochondrial RNA (1.5 μg) from normal rats (n), injured rats 1 or 7 d postinjury (i1, i7), or rats treated with pcRNA1-3 for 6 h (t) using gene-specific primers for COIII or ND5. *F*) Transcript levels of individual mitochondrial genes relative to the normal level (taken as 100 in each case), in normal (blue bars), 1 d postinjury (red bars), 7 d postinjury (green bars), or 7 d injured muscle after 6 h of treatment with pcRNA1-3 (violet bars).

hanced level in mitochondria (Fig. 1*E*), indicating processing of the pcRNA2, as previously observed in cultured cells (18).

The relative levels of various mitochondrial mRNAs, such as ND5 and COII, quantified by RT-PCR (Fig. 1*E*, *F*) were reduced following needle injury in muscle. Down-regulation occurred progressively with time; by 7 d postinjury, the levels were down to 5–30% of normal (Fig. 1*E*, *F*). An exception was apocytochrome b (CYB) mRNA, which was reduced by only ~50%.

In view of the genome-wide deficiency of mitochondrial mRNAs, we chose to administer a combination of pcRNAs 1R, 2R and 3R together encoding all the protein-coding and tRNA genes of the mitochondrial H strand (Fig. 1*A*). Administration of such a cocktail resulted in restoration of the mRNA levels to 60–85% of normal (Fig. 1*E, F*).

The global down-regulation of mitochondrial mRNAs following injury suggested a deficiency of organellar translation. Injured rats were treated with R6 and either control D-arm RNA or the pcRNA cocktail. Mitochondria were isolated from the injury site at various times thereafter and incubated with amino acid precursors under conditions favoring mitochondrial translation (22). In this *in organello* system, a general down-regulation of translation of most mitochondrial proteins was observed subsequent to injury and administration of control RNA, and some polypeptides were entirely absent (**Fig. 2*A***, left). In presence of pcRNA1-3, the normal mitochondrial translation profile was restored after 6 h of treatment, but translation efficiency was reduced at later times (Fig. 2*A*, right panel), presumably due to degradation of the delivered RNAs.

The respiratory capacity (O_2 uptake rate) of the injured muscle was stimulated 3-fold after 27 h of treatment with the pcRNA cocktail (Fig. 2*B*). Each of the 3 pcRNAs present in the cocktail contributed incrementally to respiratory capacity, but the maximal effect was produced by a combination of all 3 (Fig. 2*C*).

Intramuscular ATP levels in injured muscle were raised 5- to 6-fold on treatment with pcRNAs (Fig. 2*D*). This increase was sensitive to the complex III inhibitor AntA and the protonophore uncoupler CCCP (Fig. 2*D*), indicating the ATP elevation to be due to increased oxphos after RNA delivery.

We also estimated intracellular ROS levels (specifically that of superoxide) by quantitative MitoSox Red staining of muscle cryosections. In normal quadriceps muscle there was a low level of staining, but the level was increased ~4.5-fold in injured muscle that was either untreated or treated with control D-arm RNA (Fig. 2*E*). In the latter case, there was significant particulate staining (presumably mitochondrial) at the periphery of myofibers as well as in infiltrating cells (Fig. 2*E*). Treatment of injured muscle with pcRNAs for 12 h resulted in suppression of MitoSox staining (Fig. 2*E*), but ROS levels in-

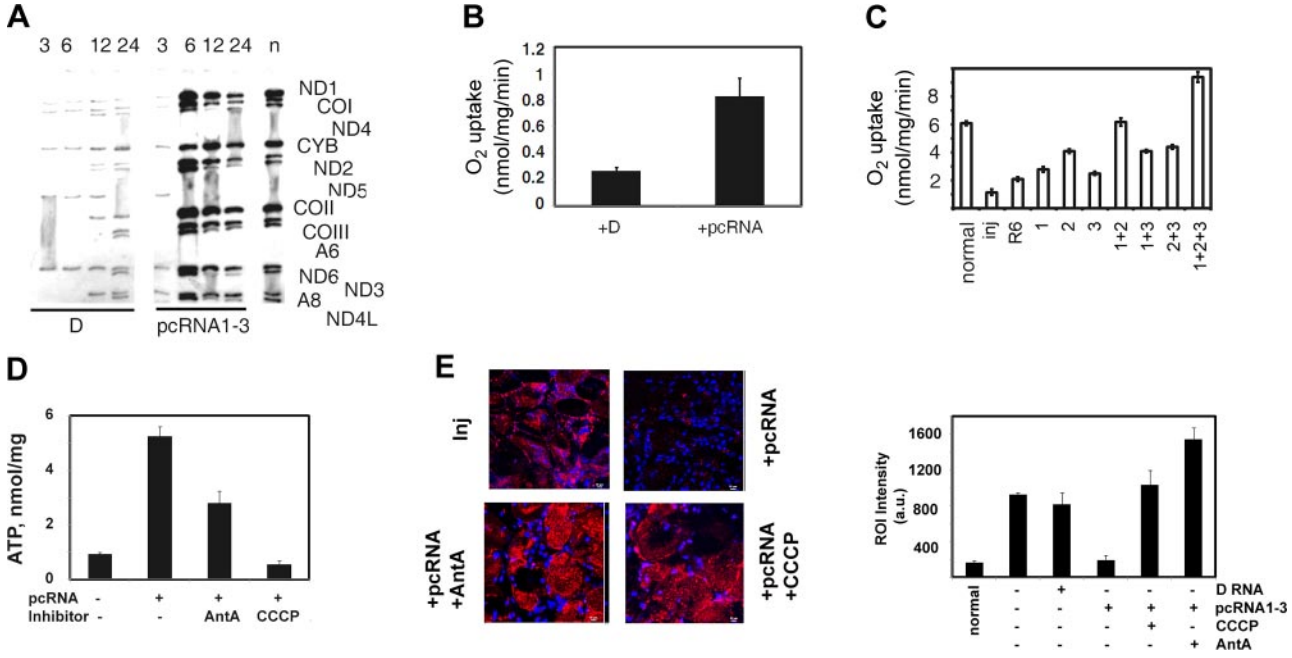

Figure 2. Restoration of mitochondrial function in regenerating rat muscle by RNA. *A*) Fluorograph of *in vitro* translation products of mitochondria from injured rat quadriceps muscle treated with a complex of R6 with D-arm RNA (left panel) or a combination of pcRNA1–3 (1 pmol each; right panel) for the indicated times (h), showing ^{35}S-labeled mitochondrial proteins (identified at right). Lane n, translation profile of mitochondria from normal muscle. *B, C*) O_2 uptake rate (state 3 respiration) of mitochondria from 6 d injured muscle treated with the pcRNA1–3 combination, or D-arm control RNA, for 27 h (*B*), or with R6 plus the indicated pcRNAs (1R, 2R, or 3R; 1 pmol each) for 3 h (*C*); the mean of 3 independent determinations is shown in each case, with SD values ranging from 0.12 to 1.2 nmol/mg/min. *D*) ATP levels in injured muscle without or with pcRNA1–3 treatment for 12 h, in the absence or presence of AntA or CCCP. *E*) Left panels: MitoSox Red staining of injured muscle after the indicated treatments. Right panel: quantification of fluorescence per field (n=10).

creased in pcRNA-treated muscle in presence of AntA, or to a lesser extent, of CCCP (Fig. 2*E*). This shows that injury results in aggravated ROS production, and that the suppression of ROS was a result of recovery of mitochondrial respiration.

Wound healing and restoration of muscle contractile function

Needle injury of the quadriceps muscle of adult rats resulted in rapid inflammation followed by a slow

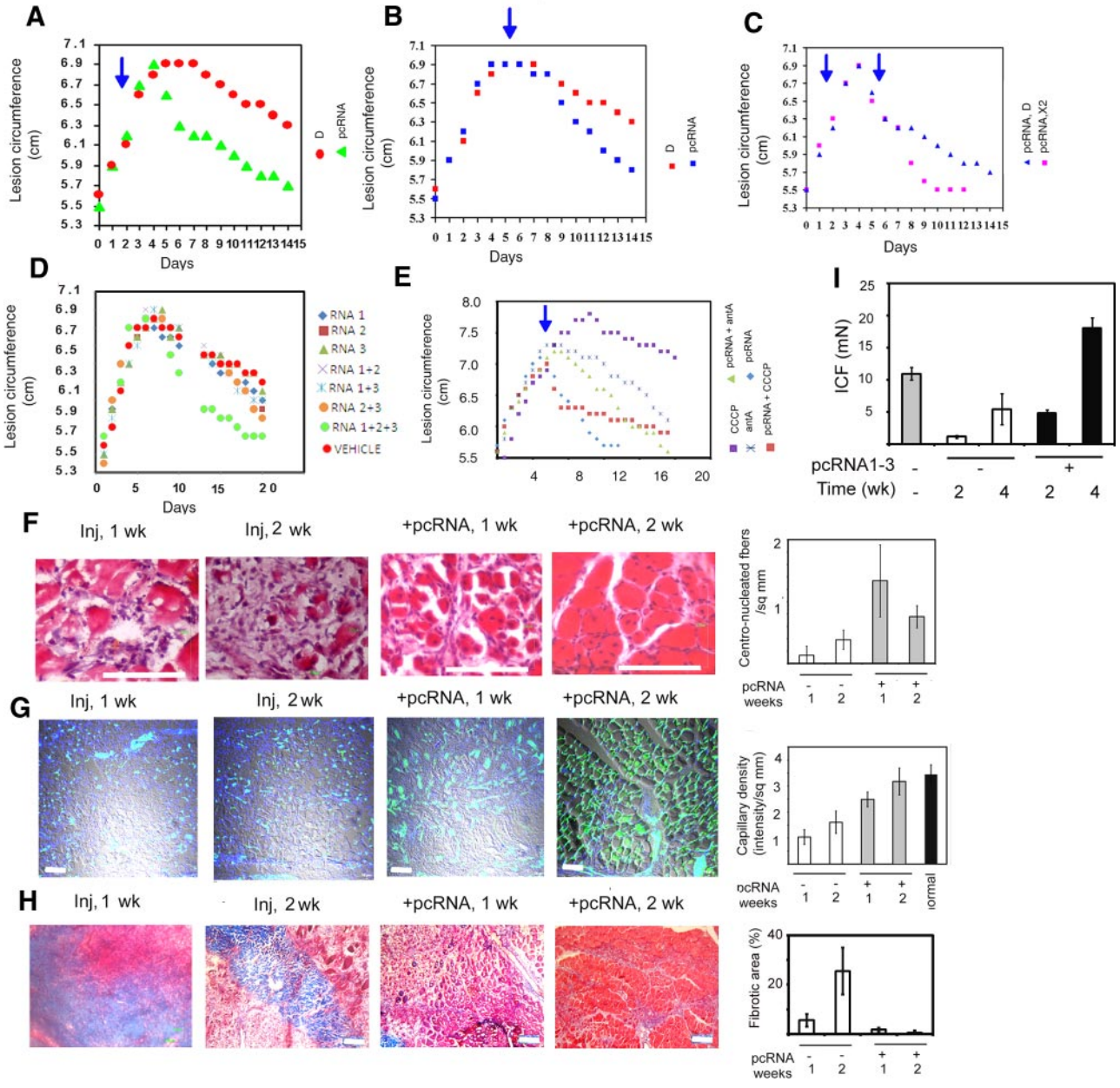

Figure 3. Enhanced wound healing in presence of pcRNAs. *A–E*) Time-dependent variations of lesion circumference of rat hindlimb after needle injury initiated at d 0, and treated with R6 plus indicated RNAs (1 pmol, blue arrow). *A*) pcRNA1-3 (green) or control D-arm RNA (red) on d 2. *B*) pcRNA1-3 (blue) or control D-arm RNA (red) on d 6. *C*) pcRNA1-3 on d 2, followed by D-arm RNA (blue) or pcRNA1-3 (pink) on d 6. *D*) Indicated combinations of pcRNA1–3 on d 6. *E*) pcRNA1-3 on d 6 followed by, 3 h later, vehicle (blue diamonds), CCCP (red squares), or AntA (gray triangles); effects of CCCP (blue squares) and AntA (blue stars) in the absence of pcRNA treatment are also shown. *F*) Hematoxylin-eosin stain of 6 d injured muscle untreated or treated with pcRNA1-3 for 1 or 2 wk. Right panel: mean number of centronuclear myofibers per square millimeter injured area in untreated or pcRNA1-3 treated injured muscle ($P<0.0001$ for 1 and 2 wk treatment). *G*) FITC-Isolectin B4 stain (green) of untreated or treated muscle merged with the DIC image to show the myofibers. Right panel; mean capillary density of untreated or treated muscle, compared to the normal (uninjured) value ($P<0.0001$). *H*) Masson trichrome stain of muscle shows intense blue regions of fibrosis. Right panel: quantification of fibrotic areas ($P<0.0003$ for 1 wk treatment; $P<0.0001$ for 2 wk treatment). *I*) ICF of normal, injured, or pcRNA-treated injured muscle 2 or 4 wk after pcRNA treatment; values are shown as means ± SD; $n = 3$. Scale bars = 100 μm.

recovery phase (**Fig. 3*A***). If the pcRNA combination was administered during the inflammatory phase (d 2), it failed to immediately arrest further inflammation, which continued at more or less the same rate, but the onset of the repair phase occurred earlier (Fig. 3*A*). Administration of the pcRNA cocktail at the peak of inflammation (d 6) resulted in acceleration of the rate of resolution by ~2-fold compared to controls: 0.140 ± 0.045 cm/d (n=4) for pcRNA *vs.* 0.069 ± 0.025 cm/d (n=4) for control (D-arm-treated) lesions (Fig. 3*B*).

The restorative effect of pcRNAs is temporary due to the turnover of the exogenous RNAs in the mitochondrial matrix (17–19). Therefore, we tested the effect of a second dose of RNA. Injection of pcRNA1R–3R on d 2, followed by a second dose on d 6, resulted in further enhancement of the healing rate (Fig. 3*C*).

We also tested the effect of the pcRNAs administered individually or in various combinations. None of the individual RNAs or pairwise combinations enhanced the healing rate as effectively as the cocktail of all three (Fig. 3*D*). This is in keeping with the genome-wide mitochondrial down-regulation, which would require a pan-genomic combination of mRNAs for effective mitochondrial restoration.

Treatment of pcRNA-treated injured muscle with mitochondrial inhibitors led to delayed wound healing. In the presence of AntA, resolution of the lesion by pcRNA was delayed, and the resolution rate was slower (Fig. 3*E*). In the presence of CCCP, which uncouples oxphos by dissipating the transmembrane proton gradient, the resolution rate was initially indistinguishable from that with pcRNA alone, but subsequently declined to control levels (*i.e.*, in the absence of pcRNA). Either inhibitor, administered alone, exaggerated the inflammation and reduced the healing rate (Fig. 3*E*). Thus, acceleration of wound healing was dependent on the recovery of mitochondrial electron transport and oxidative phosphorylation subsequent to delivery of the pcRNAs.

Histological staining of the injured tissue after 1–2 wk revealed necrotic areas and few if any myofibers; treatment with the pcRNAs resulted in the appearance of newly formed (centronucleated) myofibers, indicating myogenesis (Fig. 3*F*). The numbers of such fibers was high after 1 wk and then declined, presumably having being converted to mature fibers (with peripheral nuclei). In the presence of pcRNAs, vasculogenesis (*i.e.*, formation of the microcapillary network) was initiated by 1 wk as clusters of endothelial cells attached to myofibers, organizing around the fibers by 2 wk, but the network was not complete at this time (Fig. 3*G*; staining patterns of normal rat muscle are shown in Supplemental Figs. S4–S6). There was also a significant reduction in the fibrotic areas on administration of RNA (Fig. 3*H*).

Muscle contractility was measured *ex vivo* to reveal >50% recovery of the normal ICF after 2 wk of RNA treatment (Fig. 3*I*). By 1 mo, the ICF had recovered to a nearly 2-fold higher level compared to uninjured, untreated controls of the same age (Fig. 3*I*). These events recapitulate the processes of normal wound healing, but in an accelerated mode, and further indicate a rejuvenating effect of RNA on regenerated muscle.

Proliferation and differentiation of satellite cells *in vivo*

Regeneration of skeletal muscle involves the activation of quiescent myogenic precursor satellite cells to form myoblasts and their proliferation, differentiation, migration, and fusion to form intact myotubes or repair patches on preexisting fibers (26). We examined the expression of molecular markers relevant to these events in injured muscle treated for various times with the pcRNA cocktail plus R6; as control, the contralateral limb was injected with D-arm RNA plus R6.

Between 6 and 12 h after RNA treatment, there was evidence of cellular DNA synthesis in the form of expression of PCNA, an S-phase marker, coinciding with the appearance of cyclin D1; both proteins declined subsequently (**Fig. 4*A***). There was no such elevation in the level of either protein in injured muscle treated with control D-arm RNA. There was a coinciding peak of M-cadherin, a marker of migrating satellite cells (Fig. 4*A*). Clusters of proliferating satellite cells expressing nuclear PCNA and plasma membrane localized M-cadherin were observed between the myofibers; only a few M-cadherin-lacking cells with cytoplasmic PCNA were observed in control injured muscle (Fig. 4*B*). The yield of mononuclear cells cultured from single myofibers was increased ~2-fold in injured muscle treated with pcRNAs, compared to control RNA-treated muscle (data not shown). FACS analysis of mononuclear cells isolated from injured muscle was employed to assess the proliferation of $Pax7^+$ satellite cells. In the absence of pcRNAs, ~95% of the $Pax7^+$ cells were $PCNA^-$, indicating quiescence; after 24 h of treatment with pcRNA1-3, 60–70% of the cells were $Pax7^+$ $PCNA^+$ (Fig. 4*C*). The low percentage of proliferating satellite cells in controls is a reflection of the slow rate of regeneration under the experimental conditions (*i.e.*, multiple laceration wounds on middle-aged muscle at 6 d postinjury). It is expected that the "natural " rate of regeneration would vary inversely with age and the severity of the injury, but we have not yet investigated these aspects. The high level of ROS (Fig. 2) in injured muscle may contribute to the lack of proliferation of the satellite cells.

The increased proliferation of satellite cells in response to pcRNAs was sensitive to CCCP, showing the requirement of coupled oxphos (Fig. 4*D*). When satellite cell cultures were incubated with pcRNA1R–3R for 4 d *in vitro*, the fraction of $Pax7^+$ $PCNA^+$ cells was increased from 12–15% (for cultures incubated without RNA or with D-arm control RNA) to >75% (data not shown), showing that the proliferative effect of pcRNA1-3 persists *in vitro*. Taken together, these observations indicate that mitochondrial restoration results in rapid exit of resident satellite cells attached to

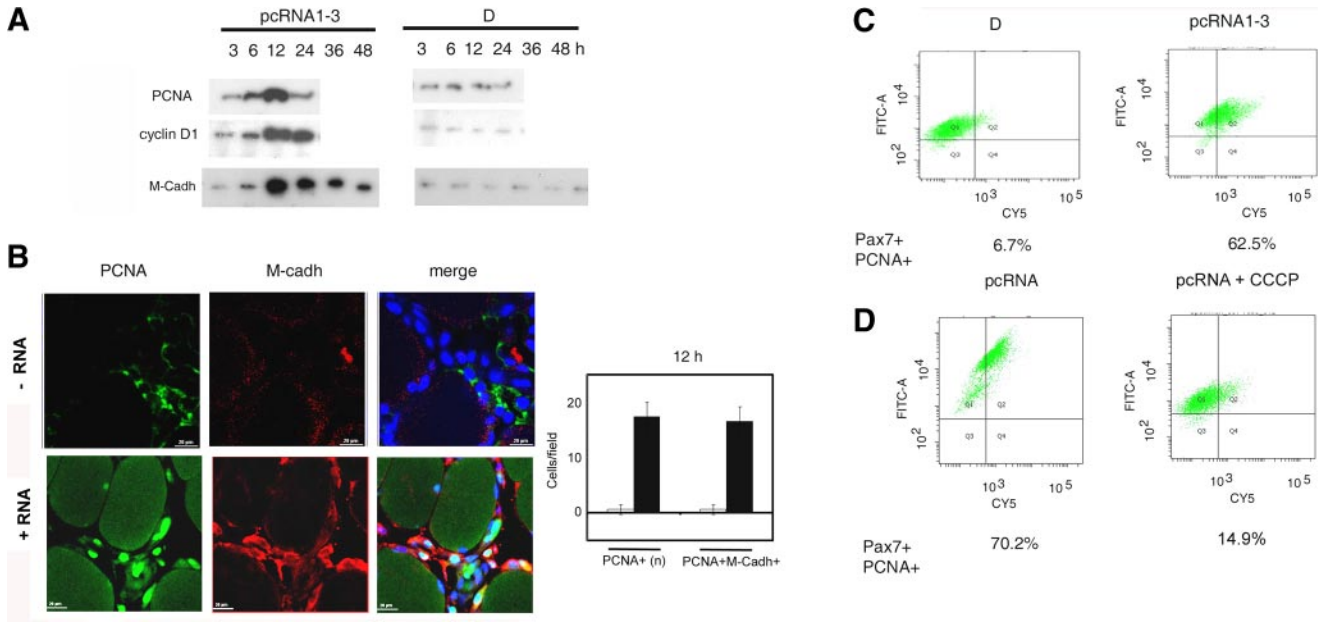

Figure 4. Proliferation of satellite cells in pcRNA-treated muscle. *A*) Western blots of injured rat quadriceps muscle treated on d 6 with pcRNA1–3 (left panel) or control D-arm RNA (right panel) for the indicated times, probed with antibodies against the indicated proteins. *B*) Confocal micrographs of 12-h untreated (top panels) or pcRNA-treated (bottom panels) injured muscle stained with antibody against PCNA (green) and M-cadherin (red); nuclei were DAPI stained. Scale bars = 20 μm. Right panel: quantification of cells with nuclear PCNA or of $PCNA^+M\text{-}cadh^+$ cells in untreated or pcRNA-treated muscle. *C, D*) FACS analysis of satellite cell fraction from myofibers of injured quadriceps muscle treated for 24 h with pcRNA1-3 or control RNA, as indicated. In *D* (right panel), 100 μM CCCP was injected 3 h after administration of pcRNA.

neighboring myofibers from the quiescent (G_0) phase to the S phase, and their proliferation between the myofibers, prior to their migration to the injury site.

Postproliferative differentiation of myoblasts was also observed in the form of time-resolved expression of myogenic regulatory factors (MRFs) belonging to the basic Helix-Loop-Helix (bHLH) family of transcription factors: Myo D, Myf5, myogenin (Myog), and MRF4 (27). In pcRNA-treated regenerating rat quadriceps muscle, up-regulation of Myo D was first observed at 12 h post-treatment and increased to a high level by 24 h, but subsequently declined (**Fig. 5*A***). A second MRF, Myf5, was also expressed in pcRNA-treated muscle as a sharp peak at 24 h (Fig. 5*A*). An established target of Myo D is Myog. In pcRNA-treated regenerating muscle, Myog was sharply induced between 12 and 24 h; *i.e.*, following Myo D induction, and high Myog levels persisted for at least 48 h (Fig. 5*A*). MRF4, which is also involved in terminal differentiation, was induced later (24–48 h) (Fig. 5*A*). In control injured muscle, no such perturbations in the levels of these MRFs were observed within this time frame (Fig. 5*A*). After 12 h of pcRNA treatment, myoblasts expressing nuclear Myo D and cytoplasmic Numb protein, which promotes commitment of myogenic precursors (28), were detected attached to, and apparently migrating on, old myofibers at the injury site (**Fig. 6*A***); few such cells were observed in control (untreated) muscle at this time (Fig. 6*A*, top panel, quantification at right).

During the later stages of myogenesis, structural proteins of the contractile apparatus, such as the myosins and troponins [troponin T (TnT)] are synthesized. Among the many isoforms of the myosin heavy chain (MHC), the embryonic form, eMHC, is induced during adult myogenesis, but disappears in mature fibers (29). In pcRNA-treated regenerating muscle, eMHC was first detectable at 24 h, and high levels persisted until at least 48 h (Fig. 5*A*). $eMHC^+$ myocytes were detectable in prefusion aggregates at 36 h (Fig. 6*B*). By 48 h, fused $eMHC^+$ myofibers and repair patches on old myofibers were apparent (Fig. 6*C*). Few such myocytes or myofibers were detectable at these times in untreated injured muscle (Fig. 6*B, C*, right).

Beginning at 2 d post-treatment with pcRNA cocktail, induction of the slow variant of TnT, TnT(s), a structural component enriched in slow-twitch myofibers, was observed (Fig. 5*A*). The level of the fast form, TnT(f), remained high and was not affected by the treatment (data not shown). In microscopic images of the regeneration site after 4 d, newly formed myotubes with central nuclei were observed, which preferentially stained for TnT(s) (Fig. 6*D*). In control injured muscle, few such myofibers were detected after 4 d (Fig. 6*D*, right).

We examined whether treatment with pcRNAs resulted in increased mitochondrial biogenesis. The mitochondrial biogenesis factor PGC1α was induced at 36–48 h post-treatment (Fig. 5*A*). The amount of skeletal muscle mtDNA relative to that of nuclear DNA was lowered after injury; in injured muscle treated with pcRNAs, the mtDNA copy number remained constant during the first 2 d, but increased significantly after 3 d; *i.e.*, in maturing myofibers (Fig. 5*B*).

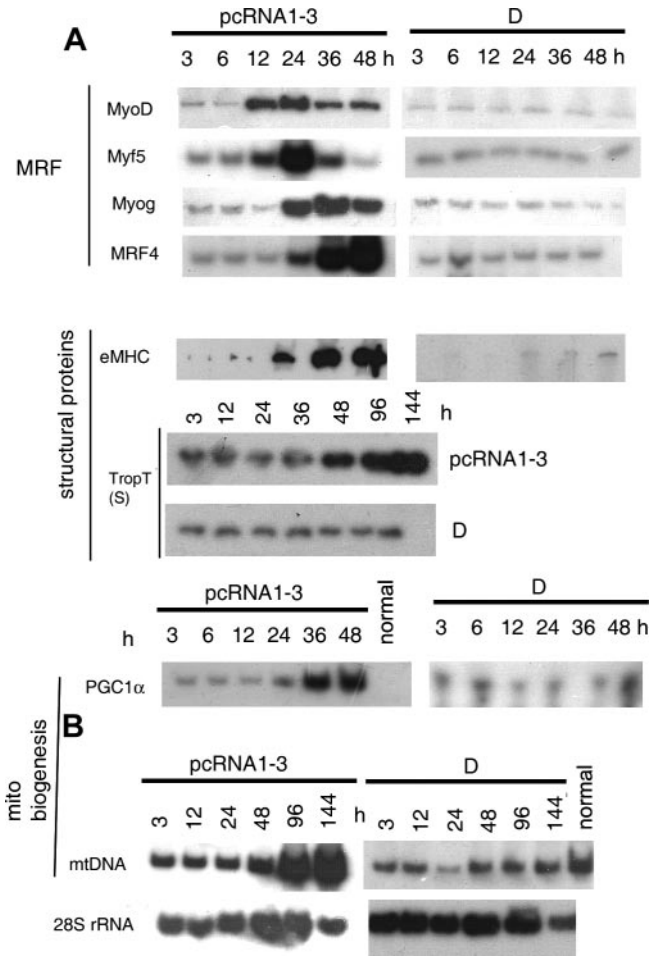

Figure 5. Postproliferative events in pcRNA-induced myogenesis. *A*) Western blots of injured muscle treated with pcRNA1-3 (left panel) or control D-arm RNA (right panel) for the indicated times, probed with antibodies against the indicated proteins. *B*) Southern blots of muscle genomic DNA probed with anti-COII or anti-28S rRNA oligonucleotide.

DISCUSSION

In this report, we show for the first time that improvement of muscle mitochondrial function through RNA delivery results in a marked improvement of myogenesis, vasculogenesis, and contractile function in injured muscle through the activation, proliferation, and differentiation of endogenous stem cells. The protocol of mitochondrial delivery is simple, efficient (effective at nanomolar RNA concentrations and transforming >80% of the mitochondria) and rapid (producing mitochondrial restoration within hours of administration), but temporary, being limited by the turnover of the RNA within mitochondria (17–19). Indeed, repeated administration of pcRNAs improved the healing rate further (Fig. 3).

The approach of endogenous stem cell activation may be compared with the implantation of exogenous hematopoietic stem cells, or of satellite cells, into regenerating muscle. In RNA-restored muscle, myogenesis was completed within a week, as opposed to several weeks in untreated toxin-injured muscle (5), or in muscle treated with $CD133^+$ stem cells from peripheral blood (15). Autologous satellite cells were shown to generate relatively low numbers of myofibers in *mdx* mice, but it is unknown whether these numbers suffice to alleviate the symptoms of Duchene muscular dystrophy (30). Similarly, the efficacy of treatment of myocardial infarction is severely limited by the low efficiency of transplanted cardiac stem cells (14). While the basis of these deficiencies is unknown, our results point to the importance of the mitochondrial function of the cultured cells as a potential contributor. If so, mitochondrial restoration of cultured stem cells *in vitro* prior to implantation could be an alternative way to improve existing procedures.

Implantation of purified stem cells with limited developmental potential results in partial regeneration; *e.g.*, $CD34^+$ or $CD133^+$ cells promote angiogenesis, their effect on myogenesis being an indirect effect of blood vessel formation (15), whereas satellite cells generate myofibers with no evidence of concurrent angiogenesis (30). Recently, low numbers of freshly isolated satellite cells embedded in a hydrogel were shown to generate myofibers in ablated mouse muscle, but there was incomplete vascularization and reinnervation even after 6 wk (31). In contrast, pcRNA treatment resulted in more than complete recovery of skeletal muscle contractile activity by 4 wk (Fig. 3). The fact that the activity of the regenerated muscle was nearly 2-fold higher than that of uninjured controls of the same age indicates a rejuvenating effect of the RNA acting through mitochondrial restoration.

Mitochondrial restoration of the entire microenvironment of the injury site provides an opportunity of resident stem cells, including satellite cells and endothelial precursor cells (EPCs), to be rapidly activated. In RNA-restored muscle, we observed myogenesis as well as vasculogenesis, and recovery of contractile function, a consequence of muscle innervation through neural regeneration (Fig. 3). However, vasculogenesis was detectably slower than myogenesis (Fig. 3), remaining incomplete after 2 wk, by which time myogenesis had been completed. The different rates of the two processes in response to mitochondrial restoration indicate that they occur independently through activation of EPCs and satellite cells, respectively. Mitochondrial restoration could also promote neural outgrowth, leading to faster innervation of the regenerated muscle and thus recovery of contractile activity.

A connection between mitochondrial function and cell differentiation has been observed in ESCs and iPSCs (11, 12). The current paradigm is that as stem cells differentiate, they switch to oxphos from a glycolytic mode of maintenance of the pluripotent state; conversely, dedifferentiation of somatic cells to iPSCs is linked to loss of mitochondrial function and switch to glycolysis. We have observed that, *in vivo*, mitochondrial activation resulted in proliferation of the resident satellite cells followed by their differentiation; thus the primary effect of mitochondrial restoration is on the

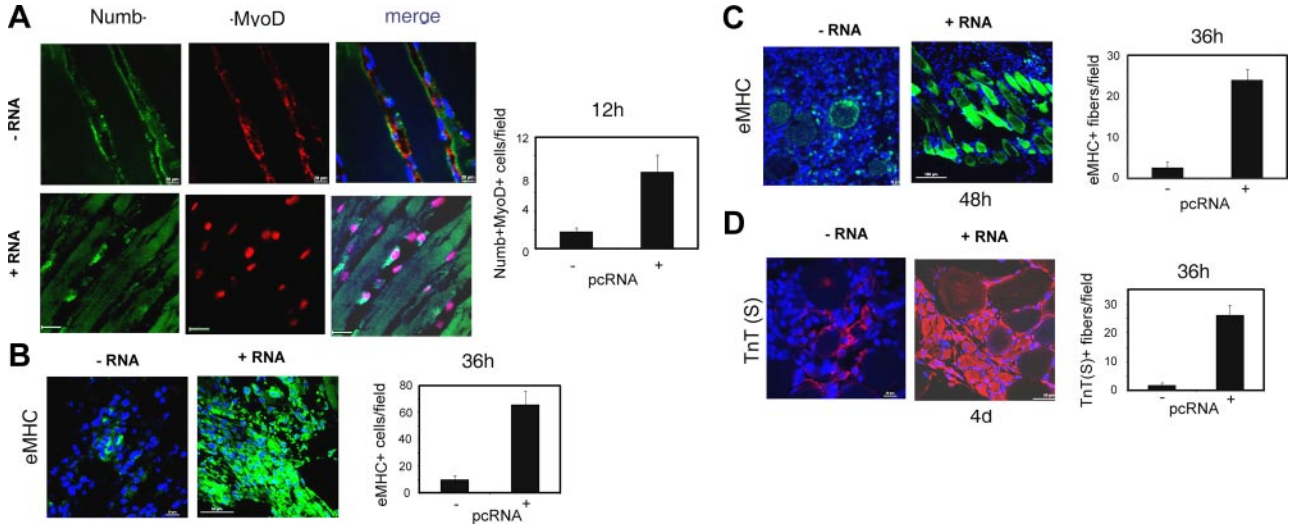

Figure 6. Formation of myoblasts and myotubes in pcRNA-treated regenerating muscle. *A*) Confocal image of myoblasts expressing cytoplasmic Numb (green) and nuclear MyoD (magenta) attached to or migrating on damaged myofibers; 12 h. *B*) Prefusion aggregates of myoblasts expressing eMHC (green); 36 h. *C*) New myotubes, and repair patches on damaged myofibers, expressing eMHC, 48 h. *D*) A repair site (96 h post-treatment) with control (left image) or pcRNA (right image) stained for slow TnT(s) (red). At bottom left of right image are aligned myoblasts lying adjacent to newly formed myotubes with central nuclei; both forms express slow troponin (red), while mature myofibers surrounding the repair site do not. Scale bars = 20 μm (*A*); 50 μm (*B*, *D*), 100 μm (*C*).

pool of differentiation-competent myoblasts. Proliferation of satellite cells is regulated by the Notch signaling pathway (28), and our preliminary results indicate activation of this pathway in pcRNA-treated injured muscle (unpublished results). The relation between mitochondrial function and Notch activation is unclear at the present time, but could be attributed to changes in the microenvironment caused by increased respiration; *e.g.*, increase in the ATP pool that would directly impact a rate-limiting enzyme with affinity for ATP, reduction in the AMP pool that senses the cellular metabolic status, increase in mitochondrial membrane potential that would activate inner membrane transporters, thus altering the cytoplasmic pools of Ca^{2+} and other signaling molecules, or exacerbation of hypoxia in the ischemic environment of the injury site with consequent activation of hypoxia-inducible factors (HIFs) and HIF target genes. Experimental discrimination between these possibilities will be instrumental in unraveling the nature of the molecular switches that connect mitochondrial function to stem cell differentiation pathways. FJ

The authors thank Tapas Chowdury for technical help, Anupam Banerjee for confocal microscopy, Uday Bandyopadhyay for oxygraph measurements, Shymal Roy for FACS analysis, and K. P. Mohanakumar for cryotome sectioning. This study was supported by the Indian Council of Scientific and Industrial Research (CSIR) Suprainstitutional Project SIP007. S.J. was a Senior Research Fellow (CSIR).

REFERENCES

1. Padfield, K. E., Astrakas, L. G., Zhang, Q., Gopalan, S., Dai, G., Mindrinos, M. N., Tompkins, R. G., Rahme, L. G., and Tzika, A. A. (2005) Burn injury causes mitochondrial dysfunction in skeletal muscle. *Proc. Natl. Acad. Sci. U. S. A.* **102,** 5368–5373
2. Cree, M. G., Fram, R. Y., Herndon, D. N., Qian, T., Angel, C., Green, J., Mlcak, M. R., Aarsland, A., and Wolfe, R. R. (2008) Human mitochondrial oxidative capacity is acutely impaired after burn trauma. *Am. J. Surg.* **196,** 234–239
3. Chen, Q., Moghaddas, S., Hoppel, C. L., and Lesnefsky, E. J. (2008) Ischemic defects in the electron transport chain increase the production of reactive oxygen species from isolated rat heart mitochondria. *Am. J. Physiol. Cell Physiol.* **294,** C460–C466
4. Grattagliano, I., Bonfrate, L., Diogo, C. V., Wang, H. H., Wang, D. Q. H., and Portincasa, P. (2009) Biochemical mechanisms in drug-induced liver injury: certainties and doubts. *World J. Gastroenterol.* **15,** 4865–4876
5. Duguez, S., Féasson, L., Denis, C., and Freyssenet, D. (2002) Mitochondrial biogenesis during skeletal muscle regeneration. *Am. J. Physiol. Endocrinol. Metab.* **282,** E802–E809
6. Lonergan, T., Brenner, C., and Bavister, B. (2006) Differentiation-related changes in mitochondrial properties as indicators of stem cell competence. *J. Cell. Physiol.* **208,** 149–153
7. Chen, C. T., Shih, Y. R., Kuo, T. K., Lee, O. K., and We, Y. H. (2008) Coordinated changes of mitochondrial biogenesis and antioxidant enzymes during osteogenic differentiation of human mesenchymal stem cells. *Stem Cells* **26,** 960–968
8. Chen, M. L., Logan, T. D., Hochberg, M. L., Shelat, S. G., Yu, X., Wilding, G. E., Tan, W., Kujoth, G. C., Prolla, T. A., Selak, M. A., Kundu, M., Carroll, M., and Thompson, J. E. (2009) Erythroid dysplasia, megaloblastic anemia, and impaired lymphopoiesis arising from mitochondrial dysfunction. *Blood* **114,** 4045–4053
9. Ramalho-Santos, .J, Varum, S., Amaral, S., Mota, P. C., Sousa, A. P., and Amaral, A. (2009) Mitochondrial functionality in reproduction: from gonads and gametes to embryos and embryonic stem cells. *Hum. Reprod. Update* **15,** 553–572
10. Sahin, E., and DePinho, R.A. (2010) Linking functional decline of telomeres, mitochondria and stem cells during ageing. *Nature* **464,** 520–528
11. Rehman, J. (2010) Empowering self-renewal and differentiation: the role of mitochondria in stem cells. *J. Mol. Med.* **8,** 981–986
12. Folmes, C. D. L., Nelson, T. J., Martinez-Fernandez, A., Arrell, D. K., Lindor, J. Z., Dzeja, P. P., Ikeda, Y., Perez-Terzic, C., and Terzic, A. (2011) Somatic oxidative bioenergetics transitions into pluripotency-dependent glycolysis to facilitate nuclear reprogramming. *Cell Metab.* **14,** 264–271

13. Hamai, N., Nakamura, M., and Asano, A. (1997) Inhibition of mitochondrial protein synthesis impaired C2C12 myoblast differentiation. *Cell Struct. Funct.* **22,** 421–431
14. Codina, M., Elser, J., and Margulies, K. B. (2010) Current status of stem cell therapy in heart failure. *Curr. Cardiol. Rep.* **12,** 199–208
15. Shi, M., Ishikawa, M., Kamei, N., Nakasa, T., Adachi, N., Deie, M., Asahara, T., and Ochi, M. (2009) Acceleration of skeletal muscle regeneration in a rat skeletal muscle injury model by local injection of human peripheral blood-derived CD133-positive cells. *Stem Cells* **27,** 949–960
16. Mahata, B., Mukherjee, S., Mishra, S., Bandyopadhyay, A., and Adhya, S. (2006) Functional delivery of a cytosolic tRNA into mutant mitochondria of human cells. *Science* **314,** 471–474
17. Mahato, B., Jash, S., and Adhya, S. (2011) RNA-mediated restoration of mitochondrial function in cells harboring a Kearns Sayre syndrome mutation. *Mitochondrion* **11,** 564–574
18. Jash, S., and Adhya, S. (2011) Suppression of reactive oxygen species in cells with multiple mitochondrial DNA deletions by exogenous protein-coding RNAs. *Mitochondrion* **11,** 607–614
19. Jash, S., Chowdhury, T., and Adhya, S. (2012) Modulation of mitochondrial respiratory capacity by carrier-mediated transfer of RNA in vivo. *Mitochondrion* **12,** 262–270
20. Mukherjee, S., Basu, S., Home, P., Dhar, G., and Adhya, S. (2007) Necessary and sufficient factors for import of tRNA into the kinetoplast-mitochondrion. *EMBO Rep.* **8,** 589–595
21. Frezza, C., Cipolat, S., and Scorrano, L. (2007) Organelle isolation: functional mitochondria from mouse liver, muscle and cultured fibroblasts. *Nat. Protocols* **2,** 287–295
22. Mahata, B., Bhattacharyya, S. N., Mukherjee, S., and Adhya, S. (2005) Correction of translational defects in patient-derived mutant mitochondria by complex-mediated import of a cytoplasmic tRNA. *J. Biol. Chem.* **280,** 5141–5144
23. Kuznetsov, A. V., Veksler, V., Gellerich, F. N., Saks, V., Margreiter, R., and Kunz, W. S. (2008) Analysis of mitochondrial function *in situ* in permeabilized muscle fibers, tissues and cells. *Nat. Protocols* **3,** 965–976
24. Kirkeby, S., Mandel, U., and Vedtofte, P. (1993) Identification of capillaries in sections from skeletal muscle by use of lectins and monoclonal antibodies reacting with histo-blood group ABH antigens. *Glycoconjugate J.* **10,** 181–188
25. Mukherjee, S., Mahata, B., Mahato, B., and Adhya, S. (2008) Targeted mRNA degradation by complex-mediated delivery of antisense RNAs to intracellular human mitochondria. *Hum. Mol. Genet.* **17,** 1292–1298
26. Le Grand, F., and Rudnicki, M. A. (2007) Skeletal muscle satellite cells and adult myogenesis. *Curr. Opin. Cell Biol.* **19,** 628–633
27. Blais, A., Tsikitis, M., Acosta-Alvear, D., Sharan, R., Kluger, Y., and Dynlacht, B. D. (2005) An initial blueprint for myogenic differentiation. *Genes Dev.* **19,** 553–569
28. Conboy, I. M., and Rando, T. A. (2002) The regulation of Notch signaling controls satellite cell activation and cell fate determination in postnatal myogenesis. *Dev. Cell* **3,** 397–409
29. D'albis, A., Couteaijx, R., Janmo, T. C., and Mira, J. C. (1989) Myosin isoform transitions in regeneration of fast and slow muscles during postnatal development of the rat. *Dev. Biol.* **135,** 320–325
30. Ikemoto, M., Fukada, S., Uezumi, A., Masuda, S., Miyoshi, H., Yamamoto, H., Wada, M. R., Masubuchi, N., Miyagoe-Suzuki, Y., and Takeda, S. (2007) Autologous transplantation of SM/C-2.6^+ satellite cells transduced with micro-dystrophin CS1 cDNA by lentiviral vector into *mdx* mice. *Mol. Ther.* **15,** 2178–2185
31. Rossi, C.A., Flaibanni, M., Blaauw, B., Pozzobon, M., Figallo, E., Reggiani, C., Vitiello, L., Elvassore, N., and De Coppi, P. (2011) *In vivo* tissue engineering of functional skeletal muscle by freshly isolated satellite cells embedded in a photopolymerizable hydrogel. *FASEB J.* **25,** 2296–2304

Received for publication January 30, 2012.
Accepted for publication June 20, 2012.